UNIVERSITY OF INSUBRIA

VARESE

DEPARTMENT OF SURGICAL AND MORPHOLOGICAL SCIENCES

- FACULTY OF MEDICINE –

Development and validation of an algorithm to predict the success of the ablation of macroreentrant atrial tachycardia

CANDIDATE:

LAURA ZOLI

Matr. N. 242622

XXIV CYCLE OF Ph.D. COURSE IN EXPERIMENTAL AND CLINICAL PHYSIOLOGY

SCHOOL OF MEDICINE

TUTORS: Chiar.mo Prof. J. A. Salerno-Uriarte, Prof. Daniela Negrini

DIRECTOR OF DOCTORAL SCHOOL: Prof. Roberto Accolla

ACADEMIC YEAR 2010-2011

INDEX

ABSTRACT

1. INTRODUCTION **1**

1.1 Atrial anatomy 1

1.2 Macroreentrant atrial tachycardia 6

1.2.1 Features of the typical atrial flutter macroreeentry 11

1.3 Non conventional electroanatomic mapping 14

1.4 Three-dimensional electroanatomic mapping (Carto system) 16

1.4.1 Preparation for the mapping 17

1.4.2 Electroanatomic mapping 18

1.4.3 Analysis of the electroanatomic maps 21

1.4.4 Activation electroanatomic map 22

1.4.5 Propagation electroanatomic map 22

1.4.6 Voltage electroanatomic map 23

1.4.7 Carto system's advantages and limitation 24

1.5 Treatment of macroreentrant atrial tachycardia based on electroanatomic mapping **25**

2. AIMS OF THE RESEARCH **28**

3. ORGANIZATION OF THE STUDY **28**

4. MATERIALS AND METHODS **29**

4.1 Patient selection criteria 29

4.2 Materials 30

4.3 Electroanatomic mapping 30

4.4 Ablation strategy 32

4.5 Follow-up 34

4.6 Statistics 34

5. RESULTS **35**

PART I

5.1 Patient population 1, mapping and ablation data 35

5.2 Comparison of the successfully and unsuccessfully treated cases in population 1: identification of independent predictors of acute and/or cumulative failure 38

PART II

5.3 Development of an algorithm to predict the difficulty of the ablation procedure 41

5.4 Population II, mapping and ablation data 42

5.5 Validation of the algorithm to predict the difficulty of ablation of macroreentrant atrial tachycardia 50

6. DISCUSSION **52**

7. REFERENCES **54**

8. ACKNOWLEDGEMENTS **59**

9. CONTRIBUTIONS **59**

Abstract

Ablation of macroreentrant atrial tachycardia (MRAT) is challenging because of complex anatomy and multiple reentrant loops. In order to define an effective ablation strategy, 3-dimensional electroanatomic mapping proved very useful. To identify predictors of ablation procedure failure may be helpful for patients treatment. In the first part of our study we analyzed into details the electroanatomical features of the reentry circuit in MRAT and we compared the characteristics of successfully versus unsuccessfully consecutive treated patients undegoing electroanatomic mapping and ablation of MRAT in order to identify variables predicting the ablation outcome. Ablation was linearly placed at the mid-diastolic isthmus (MDI) to achieve arrhythmia interruption and conduction block. Variables were analyzed for predictors of both procedural failure and cumulative failure. We demonstrated a significant difference as to the electroanatomic mapping characteristics: successfully treated cases showed a narrower target isthmus with a slower conduction velocity across the isthmus itself. In the second part of our research, we analyzed the relation between the strongest predictors of procedure outcome identified in part I (MDI width and conduction velocity across the MDI) and the chance of success of the ablation procedure. In order to analyze this relation and to predict the difficulty of the ablation procedure, we developed an algorithm and we validated prospectively the accuracy of the developed model in a second patient series.

1. INTRODUCTION

1.1 Atrial anatomy

The archetypical atrial macroreentrant atrial arrhythmia is cavotricuspid isthmus dependent counterclockwise flutter. This arrhythmia is bounded posteriorly by the crista terminalis and anteriorly by the tricuspid annulus, and uses the cavotricuspid isthmus as a critical zone of slowed conduction that supports the reentrant mechanism. These features have served to facilitate the rapid recognition and evolution of a highly successful ablation strategy for the cure of this arrhythmia. Atypical atrial flutters are not as common as peritricuspidian circuits. Their systematic study is much more recent and reentry has been demonstrated as being the mechanism but the circuits are not stereotypical like in the typical atrial flutter. It is clear that these rhythms may involve a host of functional and /or anatomic barriers, and a clearer understanding of these circuits is more than of academic interest. Description of macroreentry should be related to atrial anatomy. Noncavotricuspid isthmus dependent flutters may occurr in either the right, left, or both atria in patients with or without underlying structural heart disease. While such macroreentrant flutters frequently develop following previous cardiac surgery or ablation (particularly of atrial fibrillation), they have also been observed to occurr in the absence of prior intervention when arrhythmia is supported by spontaneous regions of conduction abnormalities or electrical silence. Anderson et al. widely revisited the atrial anatomy and the anatomy of the specialized tissues, making special reference to the descriptions given at the time of their discovery[1]. Tawara[2] likened the conduction axis to a tree, with

its roots in the atrium as the atrio-ventricular node, its trunk penetrating the fibrous atrio-ventricular septum as the bundle of His, and its peripheral branches reaching the ventricular myocardium as the ramifications of the Purkinje fibers. As described by Tawara, the transition between the atrial and ventricular segments is relatively gradual. Koch[3] shortly thereafter illustrated the landmarks with the heart as seen within the body viewed in the anatomic position, the apex of his triangle appropriately depicted in superior position, and with the orifice of the coronary sinus positioned inferiorly. The atrial border of the triangle is formed by the continuation of the commissure between the eustachian and thebesian valves into the musculature of the atrial septum. This structure is now known as the tendon of Todaro. The ventricular border of the triangle is the hinge of the septal leaflet of the tricuspid valve at the atrio-ventricular junction. When the heart is decribed as it is seen in the fluoroscopic screen of the catheter laboratory, in other words, in the anatomic position, the clinician appreciates that, when the catheter is advanced from the inferior caval vein, it passes upward as it reaches the apex of the triangle of Koch. The conduction axis is a continuous strand of histologically discrete cardiac musculature that commences in the atrial myocardium as the transitional cells and compact node, pierces the fibrous atrio-ventricular insulation to become the penetrating atrio-ventricular bundle of His, and branches on the crest of the muscular ventricular septum into the right and left bundle branches. The distal components of the axis continue to be insulated from the ventricular musculature until they reach their terminations at the peripheral extent of the network of Purkinje fibers. Within the atria, there is a

fundamental problem in the histological definition of the conduction fibers since, unlike the insulated nature of the penetrating and ventricular parts of the axis, the specialized atrial components merge with the atrial myocardium, lacking any insulating fibrous sheaths. The inputs to the atrial part of the conduction axis are made up in part of transitional cells, which interpose between the working atrial myocardium and the unequivocally histologically specialized compact atrio-ventricular node. In terms of histology, it is not possible to distinguish the cells of the distal compact node from those of the proximal penetrating bundle; the presence of the insulating collar nonetheless means that, once the axis has extended into the fibrous body, it can no longer be influenced electrically by atrial events. The compact atrio-ventricular node is in potential communication with multiple areas of atrial myocardium, with transitional cells interposed at each area. It is a gross oversimplification simply to interpret the anatomic inputs in terms of discrete "slow" and "fast" pathways. In 1906, Keith and Flack[4] identified the source of cardiac rhythm in a structure at the junction of the superior caval vein with the right atrium. When compared with the atrio-ventricular node, the sinus node has a much simpler morphology; it is a spindle-shaped structure wedged into the epicardial aspect of the junction of the musculature of the superior caval vein with that of the right atrial appendage, and with its base set against the prominent terminal crest (crista terminalis) that marks internally the site of the cavo-atrial junction. The cells of the sinus node are not insulated from the neighboring atrial cells. The atrial musculature between the sinus and atrio-ventricular nodes is made up histologically of working atrial myocardial

fibers; the myocardial walls themselves are divided into relatively narrow bands by the orifices of the veins entering the chambers, and by the fibro-elastic floor of the oval fossa (fossa ovalis). Within these muscular areas, further potential for preferential conduction is provided by the packing and orientation of the working atrial myocardial fibers. Intraatrial reentrant tachycardia often develops late after surgery for congenital heart disease: the zone of slow conduction is in the region between the atriotomy scar and a natural or acquired anatomic barrier (for instance, the inferior caval vein)[5]. Macroreentrant atrial tachycardia occurring late after surgical closure of atrial septal defects can rotate around the closure patch. There have also been reports of organized macroreentrant tachycardia occurring after pulmonary vein isolation, due to reentry occurring around iatrogenic obstacles created by ablation lesions encircling the pulmonary veins[6]. The feasibility of treating atrial fibrillation with radiofrequency ablation has revived interest in the structure of the left atrium, generally conceived as simpler in structure than right atrium. Ho et al. have reviewed the atrial septum structure (because one of the approaches to the left atrium is through the atrial septum), the orientations of the major muscular bundles from both epicardial and endocardial aspects and attempted to present the relative dimensions of the atrial chamber, the distances between the pulmonary veins and the sizes of the veins themselves as seen in the normal adult heart[7]. Like the right atrium, the left atrium can be considered as having four components: septum, appendage, vestibule, and venous component. The left atrial wall, just proximal to the vestibular component, is usually smooth and, unlike the right atrium, is

without an array of pectinate muscles. The pectinate muscles are contained mostly within the atrial appendage. The left atrium lacks a terminal crest or eustachian ridge. The major part of the left atrium is venous component receiving the pulmonary veins. The musculature of the atrial wall is composed of overlapping bundles of aligned fibers that, in the majority of the hearts, are arranged in characteristics patterns with only minor individual variations. Muscular sleeves extend into the walls of the pulmonry veins to varying distances. Electrophysiologically, nevertheless, the left atrium is just as likely as the right atrium to contribute to the perpetuation of the fibrillatory process. Should a trans-septal approach be required, the valve of the oval foramen is the only true septal structure that can be perforated without risk of exiting the heart or damaging the arterial supply to the sinus node. In about 25% of hearts, a crevice in the antero-superior rim of the oval foramen yields to allow direct access to the left atrium obliquely through the crescentic margin of the probe-patent oval fossa; at this point the catheter can be very close to the anterior wall. The rest of the left atrial wall, although more uniform in thickness than the right atrium, is thicker posteriorly and in the dome. The anterior wall can be rather thin. The presence of muscular continuity into the pulmonary veins has been confirmed both macroscopically and histologically by many investigators[8]. Electrical activity in the pulmonary veins can be recorded[9]. Recent studies suggest that the changes in orientation of the muscle fibers at the veno-atrial junctions, and within the venous walls, may have a role in altering electrical activity, especially when superimposed with stretching or fibrosis. Similarly, the criss-cross arrangement of fibers in

the atrial appendage may be significant[7]. The anatomic substrate for arrhythmogenicity , however, is not clear. Additional studies of tissues from patients with documented atrial fibrillation are necessary to evaluate the cellular changes.

1.2 Macroreentrant atrial tachycardia

Regular atrial tachycardias classically are classified into *flutter* or *tachycardia*, depending on a rate cut-off around 240 to 250 beats/min and the presence of isoelectric baselines between atrial deflections in atrial tachycardia, but not in atrial flutter[10]. However, atrial tachycardia mechanisms, defined by electrophysiologic studies and radiofrequency catheter ablation, do not correlate with ECG patterns as classically defined. It has become necessary to clarify the relations between the traditionally used terms atrial flutter and atrial tachycardia and the underlying mechanism of arrhythmia, including its anatomic bases. To attain this goal, in 2001, an Expert Group was appointed jointly by The Working Group of Arrhythmias of the European Society of Cardiology and The North American Society of Pacing and Electrophysiology to draft a proposal for a new classification of atrial tachycardias[11]. Two types of atrial tachycardia can be defined clearly based on their electrophysiological mechanisms: focal atrial tachycardia (due to an automatic, triggered, or microreentrant mechanism) and macroreentrant atrial tachycardia (including typical atrial flutter and other well-characterized macroreentrant circuits in the right atrium and left atrium. Other tachycardias (atypical atrial flutter, type II atrial flutter, inappropriate sinus tachycardia, reentrant sinus tachycardia,

fibrillatory conduction) cannot always be well classified because of inadequate understanding of the mechanism(s). Thus, the term *flutter* will refer to a continuously waving pattern on the ECG, without isoelectric baseline in at least one lead, whatever the cycle length. The term atypical atrial flutter should be defined as any tachycardia fulfilling the classic ECG definition of a continuously undulating pattern but not fitting the typical and reverse typical flutter patterns. If the flutter/tachycardia is stable enough to have its mechanism elucidated by mapping and entrainment studies, description of the mechanism should be used with or without the term atypical. The mechanism of macroreentrant atrial tachycardia is reentrant activation around a "large" central obstacle, generally several centimeters in diameter, at least in one of its dimensions. The central obstacle may consist of normal or abnormal structures and it can be fixed, functional, or a combination of the two. There is no single point of origin of activation, and atrial tissues outside the circuit are activated from various parts of the circuits. Ablation treatment of post-incisional macroreentrant atrial tachycardia and atypical atrial flutter is challenging. Short- and long-term clinical outcomes associated with catheter ablation of these arrhythmias remain lower than the rates seen in atrial flutter and other supraventricular tachycardias in patients with normal cardiac anatomy. In patients with structurally normal hearts the most prevalent type of atrial tachycardia is a macroreentrant atrial tachycardia, more specifically common atrial flutter, which is related to a right atrial macroreentrant circuit around the tricuspid annulus and is amenable to radiofrequency catheter ablation by transecting the cavotricuspid isthmus, which is delineated by the tricuspid

annulus, the coronary sinus ostium, and the Eustachian ridge adjacent to the inferior vena cava. In contrast, in patients with repaired congenital heart disease other atrial tachycardias may occur, due to existence of variable and multiple arrhythmogenic substrates, related to the underlying heart disease and or the surgical incisions. In post-incisional macroreentrant atrial tachycardia, the central obstacle of the circuit is an atriotomy scar, septal prosthetic patch, suture line, or line of fixed block secondary to radiofrequency ablation[6]. Other obstacles may include anatomic structures located in the vicinity of the scar (superior and inferior vena cava). Low-voltage electrograms characterizing areas of scar and flat bipolar recording characterizing the prosthetic patch can be observed during both sinus rhythm and atrial tachycardia. Very complex and/or multiple reentrant circuits can be seen after placement of an intra-atrial baffle (Mustard, Senning), in very dilated right atrium after a Fontan procedure, after maze surgery, and after endocardial radiofrequency ablation line for atrial fibrillation. The best characterized atriotomy macroreentrant atrial tachycardia, after placement of an intra-atrial baffle to treat transposition of the great vessels, is due to activation around an incision scar in the lateral right atrial wall[12]. Narrow passages (isthmuses) in the circuit can be found between the superior vena cava and superior end of the atriotomy scar, the inferior vena cava and inferior end of the atriotomy, the atriotomy scar and tricuspid valve, or the septal patch and inferior vena cava or tricuspid valve, or even within the scar itself. These isthmuses can be areas of slow conduction. Typical atrial flutter often is associated with right atrium atriotomy tachycardia. Not uncommonly, ablation of one will unmask the other, and

ablation of both circuits will be necessary for clinical success. Among atypical right atrial flutter, “lower loop reentry” has been the term proposed for counterclockwise reentry around the inferior vena cava where the anterior arm of the circuit is the inferior vena cava - tricuspid valve isthmus and the posterior arm is the low posterior right atrium wall with conduction across the crista terminalis. the “upper loop reentry” is characterized by a clockwise circuit, making it a variant of typical atrial flutter in which the superior turn around is lower. The “upper loop reentry” is characterized by a clockwise reentry between the tricuspid annulus and the superior vena cava. “Double wave reentry” is another macroreentry tachycardia, rapid and irregular, in which two wavefronts circulate simultaneously in the same reentrant circuit. A stable macroreentrant atrial tachycardia can originate in the left atrium. Left-sided arrrhythmia is more likely in the presence of left heart disease, such as hypertrophic myocardiopathy or mitral valve disease; in these patients, spontaneous conduction abnormalities and areas of electrical silence forming the substrate have been observed. As for the right atrium, previous cardiac surgery of left atrial and/or pulmonary veins ablation may create the necessary substrate for left atrial circuits. Several anatomic structures can be critical for the maintenance of the left atrial macroreentry: the coronary sinus, the posterior left atrium, the peri-mitral tissue, the pulmonary veins ostium and the interatrial septum. Recent studies identified electrically silent areas (defined as no recordable activity or amplitude < 0.05 mV) as the obstacle critical for the maintenance of the left atrial macroreentry. These areas (“scars”) are demonstrated in patients affected by organic heart disease,

especially involving the posterior left atrial wall[13]. Among the left atrial flutter circuits, single or double or multiple loop reentry can be identified. Although its exact prevalence among cardiac arrhythmias is difficult to establish clinically, macroreentrant atrial tachycardia is not a rare arrhythmia. It might be assumed that the incidence of macroreentrant atrial tachycardia trended toward an increase. Similarly to atrial fibrillation, this might be related to aging of the general population, which implies progressive alteration of the atrial electrical properties with development of an arrhythmogenic substrate. Moreover, the increased number of surgical and catheter-based procedures in the atria for treatment of atrial fibrillation might contribute in the coming years to an increased incidence of organized macroreentrant tachycardias occurring as a new onset arrhythmia, once atrial fibrillation has been treated successfully. Finally, the perception of an increased incidence of macroreentrant atrial tachycardia might also depend merely on our increased ability to better diagnose and treat by catheter ablation this arrhythmia. In patients with complex anatomy and multiple reentrant loops, it may be difficult to clarify the atrial activation during macroreentrant atrial tachycardia in order to define a rational ablation strategy. To this purpose, nonconventional mapping proved very effective and useful[14], [15]. In scar-related atrial macroreentrant tachycardia in patients with prior cardiac surgery and prior atrial atrial fibrillation ablation, the evaluation of surgical reports is needed. A 12 lead surface ECG with a clearly visible F (flutter) wave ideally recorded synchronously may be helpful. The identification of P wave is important to orient the electrophysiological study. During the mapping, the identification of the P wave onset is needed to

distinguish between the diastolic and the systolic period of the arrhythmia cycle. Several schematic examples of atrial flutter are presented in Fig. 1.

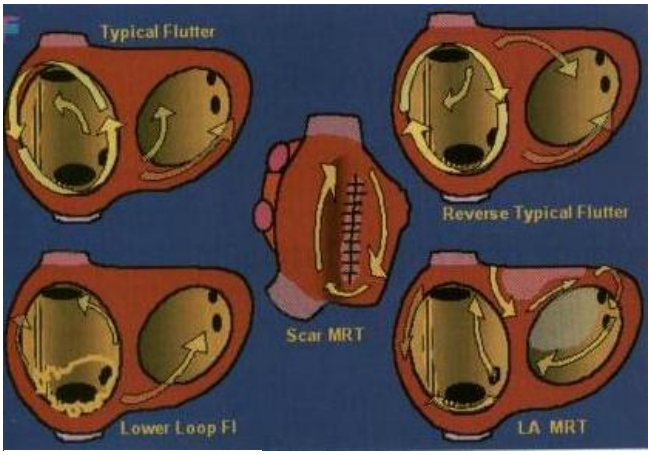

Fig. 1

1.2.1 Features of the typical atrial flutter macroreeentry

As early as 1947, when Rosenblueth developed a canine atrial flutter model by crushing endocardium between the venae cavae, it was realized that atrial flutter likely involved the propagation of a wave front around anatomically defined obstacles[16]. Canine models of atrial flutter have demonstrated the importance of anatomic obstacles in the reentry circuit[17],[18],[19],[20]. It is well established that human type I atrial flutter is a reentrant rhythm localized to the right atrium[21],[22],[23]. A protected, narrow isthmus of conduction has been identified in the low right atrium between the inferior vena cava and the tricuspid annulus[21],[24],[25],[26]. Subsequent studies suggested that this area extends across the floor of the right atrium to the os of the coronary sinus[27],[28],[29],[30],[31]. A line of block has also been observed in the lateral right atrium, extending superior from the orifice of the inferior vena cava[21],[32]. Olgin et al[33] defined

the role of right atrial endocardial structures that serve as barriers to conduction during type I atrial flutter. The Authors, using activation and entrainment mapping with anatomically determined catheter positioning guided by intracardiac echocardiography, studied the role of the crista terminalis and the eustachian ridge as anatomic barriers to conduction during typical flutter. Studying eight patients with type I atrial flutter referred to the University of California between August 1994 an December 1994, Olgin et al used the intravascular ultrasound machine to identify the endocardial structures of the right atrium (including the orifices of the venae cavae, fossa ovalis, crista terminalis, eustachian ridge, coronary sinus, and tricuspid annulus) and, along with fluoroscopy, to guide the placement of all catheters as well as to manipulate the roving catheter to specific anatomic positions. Four of the eight patients had no structural disease with normal left ventricular functional and atrial size; three patients had coronary artery disease and previous myocardial infarctions; one patient had a prior aortic valve replacement for aortic insufficiency. Two patients had ejection fraction of less than 45%; left atrial enlargement was present in only four patients, and right atrial dimensions were normal in all patients, as determined by surface echocardiography. All patients failed at least three antiarrhythmic drugs, and at least one had DC cardioversion attempted before the procedure. Three sets of results are provided that demonstrate that the crista terminalis and eustachian ridge are barriers to conduction during flutter. First, split potentials were recorded along the length of the crista terminalis - with opposite activation sequences of each component - and across the eustachian ridge.

Second, activation mapping demonstrated that sites determined by intracardiac echocardiography to be just anterior to the crista terminalis and the eustachian ridge were activated significantly later than sites determined by intracardiac echocardiography to be just posterior to these structures. Third, entrainment mapping identified sites determined by intracardiac echocardiography to be just anterior to the crista terminalis and the eustachian ridge as within the reentrant circuit, whereas sites determined to be just posterior to these structures were identified as not being within the circuit. These data indicate that the flutter wavefront is directed inferiorly along the trabeculated right atrium anterior to the crista terminalis into a narrow isthmus between the eustachian ridge and the tricuspid annulus and then medially between these two structures to exit near the coronary sinus os. Using the intracardiac echocardiography, Olgin et al demonstrated, conclusively, that the crista terminalis is the anatomic structure that acts as the barrier to conduction. The study also demonstrated that the eustachian ridge forms a barrier to conduction during atrial flutter in the low right atrium; it, along with the tricuspid annulus, forms the borders of a narrow isthmus of conduction. The area of the low right atrium between the tricuspid annulus and the inferior vena cava has been previously demonstrated to be a critical area in atrial flutter[21,24,25,28,31,34]. However, until the study of Olgin et al, the anatomic features that delineate this, and in particular the role of the eustachian ridge, were not completely known. Using the intracardiac echocardiography, Olgin et al identified the eustachian ridge as the anatomic correlate of this line of block extending from the inferior vena cava to the

coronary sinus os. From the activation maps obtained in the study of Olgin et al, typical atrial flutter occurs in a counterclockwise rotation. From the coronary sinus os, the flutter wave passively activates the interatrial septum and left atrium. After this, the trabeculated right atrium anterior to the crista terminalis is activated, directing the impulse into the narrow isthmus of slow conduction between the eustachian ridge and tricuspid annulus.

1.3 Non conventional electroanatomic mapping

Electrophysiologic testing and radiofrequency ablation have evolved as curative measures for a variety of rhythm disturbances; as experience in this field has grown, ablation is progressively being used to address more complex rhythm disturbances. Paralleling this trend are technological advancements to facilitate these efforts, including electronatomic mapping. “Electroanatomic mapping” or cardiac mapping is the process of collecting and displaying information gathered from cardiac electrograms. From the earliest days of documenting the signals that represent the electrical activity of the heart, there has been some method of deriving information from these recordings. With the advent of computer technology, medical inventors have furthered the capabilities both the recording and display of cardiac electrograms during the electrophysiologic procedures. The systems of today have advanced these functions to the point where the enterity of electrical activation within a single chamber can be recorded and displayed in a single beat. The function of a mapping system is to provide a tool that allows the user to achieve results that can not otherwise be achieved using coventional

techniques. At present, several different electroanatomic mapping systems utilizing various technologies are available to facilitate mapping and ablation. Use of these systems has been shown to reduce fluoroscopic exposure and radiation dose, with less significant effects on procedural duration and success rates. Among the data provided by electroanatomic mapping are chamber reconstruction, tagging of important anatomic landmarks and ablation lesions, display of diagnostic and mapping catheters without using fluoroscopy, activation mapping, and voltage (or scar) mapping. Several electroanatomic mapping systems have specialized features, such as enhanced ability to map non-sustained or hemodynamically unstable arrhythmias, ability to display diagnostic as well as mapping catheter posistions, and wide compatibility with a variety of catheters. Each electroanatomic mapping system has its strenghts and weaknesses, and the system chosen must depend upon what data is required for procedural success (activation mapping, substrate mapping, cardiac geometry), the anticipated arrhythmia, the compatibility of the system with adjunctive tools (i.e. diagnostic and ablation catheters), and the operator's familiarity with the selected system. While electroanatomic mapping can offer significant assistance during an electrophysiologic procedure, their incorrect or inappropriate application can substantially hamper mapping efforts and procedural success, and should not replace careful interpretation of data and strict adherence to electrophysiologic principles.

1.4 Three-dimensional electroanatomic mapping (CARTO system)

The CARTO mapping system (Biosense, Diamond Bar, CA, USA) utilizes a low-level magnetic field (5 x 10^{-6} to 5 x 10^{-5} Tesla) delivered from three separate coils in a locator pad beneath the patients (Fig. 2).

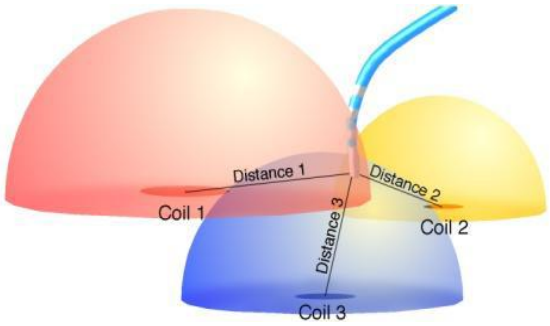

Fig. 2 Illustration demonstrating operation of the Biosense CARTO electroanatomic mapping system. Three separate coils emit a low-level magnetic field, diagrammatically represented by color-coded hemispheres. The field strenght from each coil is measured by a sensor within the tip of a specialized mapping/ablation catheter, and its position relative to each coil is then triangulated.

The magnetic field strenght from each coil is detected by a location sensor embedded proximal to the tip of a specialized mapping catheter. The strenght of each coil's magnetic field measured by the location sensor is inversely proportional to the distance between the sensor and the coil. Hence, by integrating each coil's field strenght and converting this measurement into a distance, the location sensor (and therefore, catheter tip location) can be triangulated in space[35]. The mapping catheter has proximal and distal electrode pairs, and a tip electrode capable of radiofrequency energy delivery. This catheter can be moved along a chamber's surface to record local endocardial activation times for arrhythmia mapping, while simultaneously recording location points to generate 3D chamber geometry. Validation studies have shown CARTO to have substantial accuracy in

navigating to single points, in returning to prior ablation sites, and in creating a desired length of ablation line[36]. Electrograms recorded from the specialized mapping (Navistar) catheter showed excellent correlation with recordings from standard electrophysiologic catheters. Human validation studies have shown a similar level of spatial precision and accuracy, and realistic reconstruction of chamber geometry and electroanatomic activation during arrhythmia mapping[37]. Advantages of CARTO include accurate representation of chamber geometry and the capability of generating activation maps and playable propagation maps. It also has the capability to record locations of important anatomic landmarks (such as the bundle of His), areas of electrical scar (to create voltage/scar maps) and vessels (coronary sinus, pulmonary veins). CARTO also allows recording ablation lesion location facilitating creation of ablation lines. Disadvantages include requiring the use of a specialized (NaviSTAR) catheter, inability to easily relocate a displaced reference catheter, somewhat orthogonal appearance to chamber geometry (as when a small number of location points are stored), and the inability to record or display the location of diagnostic/reference catheter.

1.4.1. Preparation for the mapping

Prior to arrhythmia mapping, a stable location reference must be established. This is accomplished by placing the location magnet, a triangular apparatus containing three magnetic coils, beneath the patient and the table. The location of this magnet must be aligned anywhere inside a defined circumference at the start of the procedure. A reference patch is affixed to the patient's back roughly overlying the cardiac chamber of interest. Should the location reference magnet or patch

become displaced during the procedure, their original location is recorded by CARTO to allow proper repositioning. This allows for accurate tracking of mapping catheter position, consistency of anatomic landmark and ablation lesion locations, and precise reconstruction of chamber geometry (Fig. 3, 4).

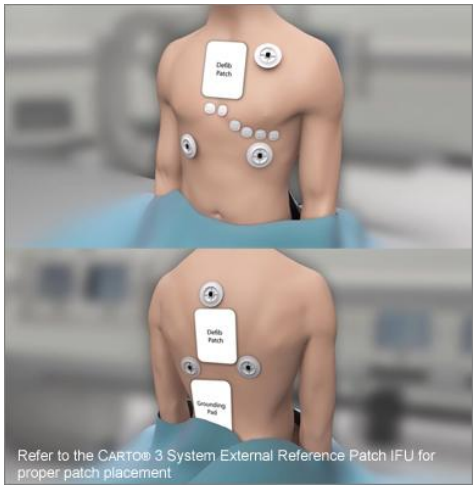

Fig. 3. CARTO 3 System external reference patch for proper patch placement

Fig.4. CARTO 3 electroanatomic mapping system

1.4.2 Electroanatomic mapping

Once the location reference has been stably situated, an appropriate timing reference and window must be selected. The timing reference is any arbitrarily selected recording (intracardiac electrogram or surface ECG lead) representative of activation of the chamber of arrhythmia origin (i.e. proximal coronary sinus atrial intracardiac electrogram chosen for mapping atrial tachycardia). Intracardiac electrograms are often selected as the timing reference as these are generally more consistent in appearance and precise in timing than surface ECG recordings, and consequently, are more reliable. Any component of the reference electrogram may be chosen for a timing reference, including maximum (peak positive) deflection, minimum (peak negative) deflection, maximum upslope (dV/dT) or maximum downslope. The proximal /mid coronary sinus electrodes are often selected as a

timing reference as the atrial intracradiac electrogram in these poles are often of greater amplitude and fidelity than their ventricular counterparts. The timing window refers to the range of activation times surrounding reference intracardiac electrogram activation. Proper timing window definition requires accurate determination of the underlying tachycardia mechanism (focal versus macroreentrant tachycardia). Once the correct tachycardia mechanism has been diagnosed, the timing window may be defined to include the extremes of cardiac activation preceding and following reference intracardiac electrogram. In a macroreentrant atrial tachycardia, the chamber of interest is electrically activated during the entire cycle of the arrhythmia. Using a coronary sinus atriogram as reference signal, the duration of the window of interest corresponds to the interval of the arrhythmia cycle considered for activation and voltage mapping. For each macroreentrant atrial tachycardia morphology, the backward and forward intervals of the window of interest are calculated according the following formulas:

$$\text{Backward interval} = (TCL - DUR^{PW}) / 2 + \text{interval}^{PWonset\text{-}ref}$$

$$\text{Forward interval} = (TCL - \text{Backward interval}) * 0{,}90$$

where DUR^{PW} is the duration of the surface P-wave during MAT (interval "a" in Fig.5), and $\text{interval}^{PWonset\text{-}ref}$ is the interval between the onset of the P wave and the reference signal (interval "b" in Fig. 5), which has a negative value when the reference signal precedes the P-wave onset. The P-wave onset and

duration is measured on the 12-leads synchronously displayed at a sweep speed of 100 mm/s.

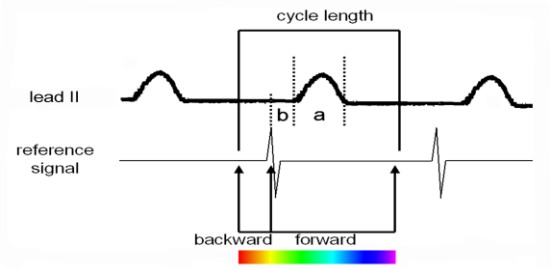

Fig. 5 Setting the window of interest

Using this formula, the onset of the window of interest is set in mid-diastole, and its duration spans between 90 and 95% of the total cycle length. As a consequence, in the color-coded activation map, red and orange identify mid- and late-diastolic activation, respectively, and dark blue and purple identify early- and mid-diastolic activation, respectively. The remaining colors identify areas of systolic activation. The interface between the red area and the purple area identifies the mid-diastolic activation isthmus of the reentrant circuit (Fig. 6).

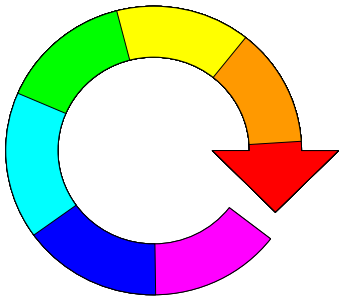

Fig. 6 "Early meets late"

Mapping is continued until a complete electroanatomic reconstruction is obtained and the interval between the earliest and latest activated sites equalles or is close to the total cycle length. The CARTO system provides location mapping features capable of recordings sites of anatomic relevance, areas of low endocardial voltage representing scar, and areas of ablation. Structures such as the bundle of His can be tagged to prevent inadvertent energy delivery resulting in conduction impairment when ablating tachycardias originating in this region. Vessels such as the coronary sinus and pulmonary veins may also be marked to provide spatial orientation to assist mapping efforts. Scar mapping can also achieved by tracing the endocardial surface and recording the amplitude of local potentials.

1.4.3 Analysis of the electroanatomic maps

Sequential recordings of several points by dragging the catheter along the endocardium allows a real-time construction of a 3D activation map. In a 3D reconstruction, the electric activation can be showed in activation maps, propagation maps and uni/bipolar voltage maps. The CARTO system calculates the volume of each cardiac chamber studied in the electroanatomic map. The volume of the cardiac chamber calculated by the electroanatomic mapping can differ from that calculated by other techniques (because affected by the cardiac rhythm) and the reconstruction of the atrial chamber can be influenced by the pressure exerted by the catheter tip on the endocardium.

1.4.4 Activation electroanatomic map

In the color-coded activation map, red and orange identify mid- and late-diastolic activation, respectively, and dark blue and purple identify early- and mid-diastolic activation, respectively. The same color characterizes the circuit areas with the same activation time (Fig.7). The electroanatomic activation map visualizes the entire arrhythmia circuit, showing a typical "head-meets-tails" pattern and clearly identifies the mid-diastolic critical isthmus.

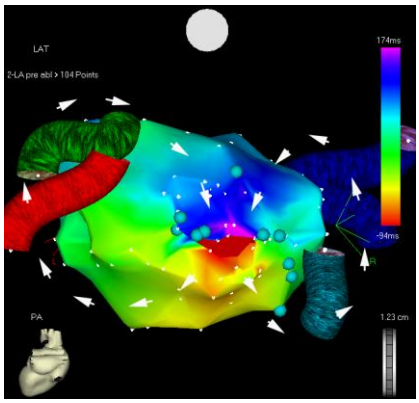

Fig. 7. Activation map of a dual loop left macroreentrant atrial tachycardia with reentry around the pulmonary veins ostia

1.4.5 Propagation electroanatomic map

Propagation maps can also be constructed and played back from data obtained through activation mapping, demonstrating spread of activation throughout a cardiac chamber during arrhythmia. The propagation front is visualized like a red band moving from the earlier activated area to the latest one (Fig. 8). The red band widht represent a range of twenty ms of the cardiac cycle. The band is large in the myocardial areas characterized by

fast propagation and narrow in the areas presenting a conduction impairment.

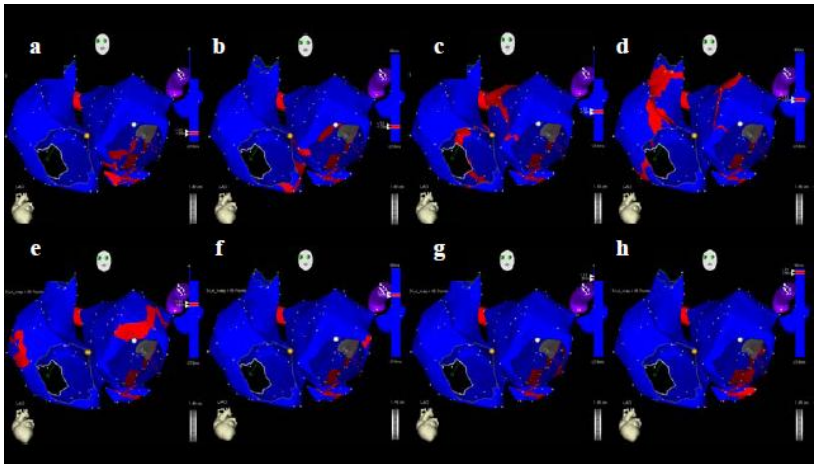

Fig. 8 a, h. Propagation map of a left atrial flutter with left atrial clockwise activation and right atrial activation from coroanry sinus

1.4.6 Voltage electroanatomic map

The voltage map is constructed using unipolar or bipolar electrograms. In this map, the lowest voltage amplitude areas are represented by red and yellow color, while dark blue and purple show high voltage areas (Fig. 9). Unfortunately, the voltage map is strictly dependent on the contact between the catheter and the endocardial surface. Bipolar voltage should be preferred because less affected by far-field arising from other cardiac chambers or next areas, but it depends on dipole orientation. However, the bipolar voltage amplitude seems to be related with the myocardial thickness and electrical viability in the examined areas. Areas with bipolar voltage (biVolt) ≤ 0.05 mV are considered electrically silent.

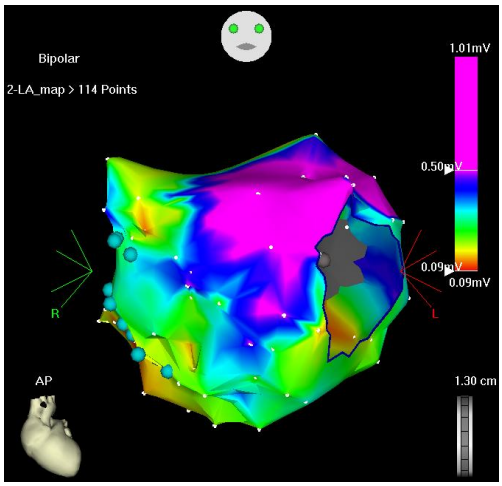

Fig. 9. Left atrium bipolar voltage map: the purple areas present normal voltages

1.4.7 CARTO system's advantages and limitations

The main advantage deriving from CARTO system consist in exact electroanatomic reconstruction of the chamber of interest, allowing more accurate recording and targeting for ablation of sites suspected to be tachycardia origin than with fluoroscopy only. Chief among advantages deriving from use of CARTO system is the electroanatomic mapping's ability to allow catheter positioning without the use of fluoroscopy, a distinct advantage for both patient and operator. Fluoroscopy time and radiation dose are indeed reduced with electroanatomic mapping when compared to conventional mapping strategies. Analyzing mapping sites homogeneously distributes in the atrial chamber and the electrical activation observed in each site, the chronology of the entire macroreentry circuit is reconstructed and the mid-diastholic isthmus is identified. High-density mapping is performed in and around the mid-diastholic isthmus in order to definiy precisely its limits

and width in order to plan the ablation strategy. The major limit of CARTO system is related to point by point mapping in order to obtain 3D-reconstruction, resulting in prolonging procedure time. Errors deriving from an incorrect acquired map may lead to an erroneously diagnosed arrhythmia mechanism, inaccurate site of tachycardia origination, or creation of a confusing, unhelpful activation map. Such errors may counteract any possible benefit offered by electroanatomic mapping and may ultimately increase fluoroscopic exposure. A second limit of electroanatomic mapping is the necessity of a sufficient stable tachycardia cycle during mapping to obtain point by point information.

1.5 Treatment of macroreentrant atrial tachycardia based on electroanatomic mapping

It might be assumed that the incidence of macroreentrant atrial tachycardia trended toward an increase. Diagnosis and ablation of this arrhythmia remains challenging and, in some cases, it may result in a lenghty procedure or failure. This has an impact on the clinical management of these patients, since pharmacologic therapy may have limited efficacy for both rhythm and rate control of this arrhythmia, usually highly symptomatic. In patients with complex anatomy, relevant organic cardiopathy and multiple reentrant loops, it may be difficult to clarify the atrial activation during macroreentrant atrial tachycardia in order to define a rational ablation strategy. To this purpose, 3-dimensional electroanatomic mapping proved very effective and useful. Using CARTO electroanatomic mapping and virtually reconstructing the

chamber of interest, we can identify the abnormal myocardial areas in order to relate these areas with the arrhythmia mechanism and guide the ablation procedure. CARTO electroanatomic mapping is an useful adjunctive tool when approaching a target arrhythmia. In order to reconstruct the chronology of the entire macroreentry circuit and to identify the mid-diastolic isthmus (MDI), a specific setting of the window of interest is used. By doing so, each color in the activation color-code scale represent a specific chronology, with red and orange identifying the mid-and late-diastolic activation, respectively, dark blue and purple identifying early-and mid-diastolic activation, respectively, while the remaining colors identify areas of systolic activation. As a consequence, the mid-diastolic isthmus is identified at the interface between the red and the purple colors and magnified by the dark red band, automatically interposed by the system. Performing homogeneous mapping in the chamber of interest, we can clarify the electrical activation, identify the critical isthmus and plan the ablation strategy. If the macroreentry is located in the left atrium, the right atrial activation has systolic chronology and earliest activation of the left atrium is recorded anterior from the septum, where anatomically the bundle of Bachamann is located and a transseptal puncture is necessary to perform left atrial mapping. If the macroreentry is located in the right atrium, before ablation procedure, electroanatomic mapping allows for marking of structures such as the sinus node and the atrio-ventricular node so that they may be avoided. In patients with post-incisional macroreentrant atrial tachycardia and left atrial flutter, irrigated-tip catheters are preferred because, in relation to the resistance of the substrate, they allow delivery of higher energy than conventional

catheters. Ablation with irrigated-tip catheter is generally performed in temperature control mode with a maximum preset temperature of 43°C and a maximum preset power of up to 50 W. The maximum application duration is preset at 60 seconds. Extension of mid-diastolic isthmus (target of the ablation procedure) strictly relates with length procedure and less need for repeated procedures. During radiofrequency energy delivery, if arrhythmia interruption with resumption of sinus rhytm occurs, the procedure is performed during sinus rhythm in order to obtain complete lesion in the mid-diastolic isthmus area identified as critical for the manteinance of the reentry[38]. In some cases, a conversion of a tachycardia morphology in a new one is possible, requiring mapping of the new morphology setting a new window of interest. This mapping and ablation method was described and validated in the multicenter prospective study named SWEET (Setting the Window of interest in macrorEEntrant Tachycardia)[15.] The study examined 65 patients and 81 macroreentrant atrial tachycardia/atypical atrial flutter morphologies. Twenty patients showed no evidence of structural heart disease, the remaining 45 showed congenital or acquired heart disease. Approximately 50% of the population was suffering for post-incisional arrhythmia (patients with prior corrective surgery in the context of congenital heart disease) or atypical atrial flutter after left atrial ablation for atrial fibrillation. In 97% macroreentrant atrial tachycardia morphologies examined, the electroanatomic map visualized the entire arrhythmia circuit, showing a typical “head-meets-tail” pattern and clearly identifying the mid-diastolic isthmus between anatomic boundaries, lines of double potentials, and/or

electrically silent areas. 93% of tachyarrhytmias was abolished by radiofrequency energy delivery at the mid-diastolic isthmus and the acute success was confirmed in a mid- and long-term follow-up.

2. AIMS OF THE RESEARCH

Aims of the present research was:

- analyze into details the electroanatomical fetaures of the circuit in macroreentrant atrial tachycardias/atypical atrial flutters
- identify predictors of ablation procedure outcomes based on the comparison between successfully and unsuccessfully treated consecutive cases
- development of an algorithm to predict the difficulty of the ablation procedure
- validate prospectively the accuracy of the algorithm in a second patient series

3. ORGANIZATION OF THE STUDY

The present study was organized in two different steps. In part I, fifty-two consecutive patients with 56 macroreentrant atrial tachycardias (MRAT) undergoing electroanatomic mapping and radiofrequency ablation were included. Ablation was linearly placed at the mid-diastolic isthmus (MDI) to achieve arrhythmia interruption and conduction block. Variables were analyzed for predictors of both procedural failure and cumulative failure (procedural failure + early recurrences). In part II, we analyzed the relation between the strongest

predictors of procedure outcome identified in part I of the research and the chance of success of the ablation procedure, developing an algorithm to predict the difficulty of the procedure. In order to test the effect of both the strongest outcome predictors of macroreentrant atrial tachycardia ablation, we applied a multiple linear regression. In the end, we validated prospectively the accuracy of this algorithm in a second series of patients who underwent electroanatomic mapping and ablation procedure for macroreentrant atrial tachycardias/atypical atrial flutter.

4. MATERIALS AND METHODS

4.1 Patient selection criteria

Consecutive patients with symptomatic sustained macroreentrant atrial tachycardia (MRAT) undergoing catheter ablation at our institution were considered. Patients with intracardiac thrombus detected at routine preprocedure transesophageal echocardiography were excluded. Morphologies with a P-wave-pattern of typical atrial flutter in which a peritricuspid isthmus-dependent circuit was confirmed by intracavitary conventional mapping were excluded, since in these cases ablation strategy is obvious. Conversely, morphologies with a P-wave pattern different from typical or reverse atrial flutter were included, even if electroanatomic mapping (EAM) identified the cavotricuspid isthmus as the critical isthmus, since in these so-called pseudo-atypical atrial flutters detailed mapping data are crucial to plan a successful ablation strategy. Antiarrhythmic drugs were withdrawn five half-lives before the procedure, except for amiodarone. If

appropriate, oral anticoagulant was administered in the weeks before the procedure and replacedby administration of low molecular weight heparin 48 hours before the procedure. The study was approved by institutional review board and all patients gave written informed consent.

4.2 Materials

Electroanatomic mapping was performed using CARTO system (Biosense Webster Inc., Diamond Barr, CA, USA), particularly CARTO Xpress, XP and the last model, CARTO 3, in association with conventional polygraphs. We used 7.5 F 3.5 mm tetrapolar bidirectional irrigated-tip catheters (Navistar Thermocool 8F, Biosense Webster Inc., Diamond Bar, CA, USA) [Fig. 10].

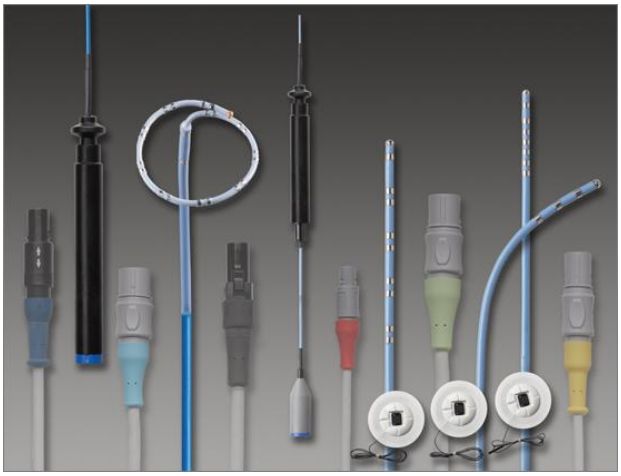

FIG. 10 Catheters and patches commonly used during CARTO electroanatomic mapping

4.3 Electroanatomic mapping

EAM (CARTO XP, Diamond Bar, CA, USA) was commenced in the right atrium and extended to the left atrium if a right-sided circuit was excluded. In

order to reconstruct the chronology of the entire macroreentry circuit and to identify the mid-diastolic isthmus (MDI), a specific setting of the window of interest was used, as previously described[15.] As a consequence of this setting of the window of interest, the MDI was identified at the interface between the red and the purple colors and magnified by the dark red band, automatically interposed by the system (fig.11). If necessary, the reentry course and the location of the critical isthmus were validated by entrainment mapping. Mapping sites were homogeneously distributed in the atrial chamber and high-density mapping was performed in and around the MDI in order to define precisely its limits and width. Areas with bipolar voltage (biVolt) ≤ 0.05 mV were considered electrically silent. Sites with double potentials separated by > 50 ms of isoelectric line were considered areas of local conduction block and activation detour and tagged in blue. Reentry was defined as double loop, when activation long each loop spanned at least 90% of the CL. The atrial volume was automatically given by the system. The width of the MDI was calculated using the electronic ruler of the system. The average peak-to-peak biVolt in the MDI was calculated for each MRAT. Conduction velocity (CV) in the MDI and in 3 segments of the outer loop in the direction of the propagating wavefront was manually calculated for each morphology. In order to obtain accurate measurements, only differences in activation in sites < 25 mm apart, in a noncurvilinear region were taken into account. According to prior reports, values of conduction velocity < 40 cm/sec were considered abnormally slow, whereas those > 60 cm/sec normal[39],[40].

Fig. 11

Activation electroanatomic map: scar areas are tagged in grey color

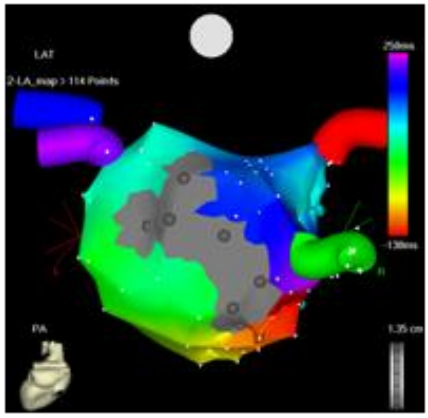

4.4 Ablation strategy

As first option, linear ablation was aimed at the MDI to achieve arrhythmia termination and conduction block in this area, as demonstrated by double potentials separated by isoelectric line with consistent change of propagation during sinus rhythm or atrial pacing from an appropriate site and/or disappearance of electrical potentials in the target isthmus and the surrounding areas. In case the characteristics of the MDI were potentially unfavorable for ablation (wide isthmus with preserved CV and biVolt amplitude), an alternative ablation strategy was considered, focusing on anatomic isthmi critical for reentry. In these cases, the alternative ablation strategy was preferred if the characteristics of the alternative isthmus (or isthmi in cases of double-loop reentry with each loop targeted separately) were better than those of the MDI in term of width, access by ablation catheter, CV, and biVolt amplitude. As previously described, a 7.5F 3.5 mm irrigated-tip catheter (Navistar Thermocool, Diamond Bar, CA, USA) was used with a power setting of 35 W, cut-off temperature of 43◦C, a flow rate during energy delivery of 30 mL/min, and application duration of 60 seconds.

In areas of preserved voltage (> 0.5 mV), power was increased up to 45 W with no change in the remaining parameters. After MRAT termination by ablation and achievement of conduction block along the target isthmus, electrical stimulation was performed to evaluate inducibility of other arrhythmias. If noninducibility persisted after 30 minutes from ablation termination, the procedure was completed. If the target arrhythmia was not terminated and alternative strategies were unsuccessful or unfeasible, the arrhythmia was electrically cardioverted and the procedure terminated.

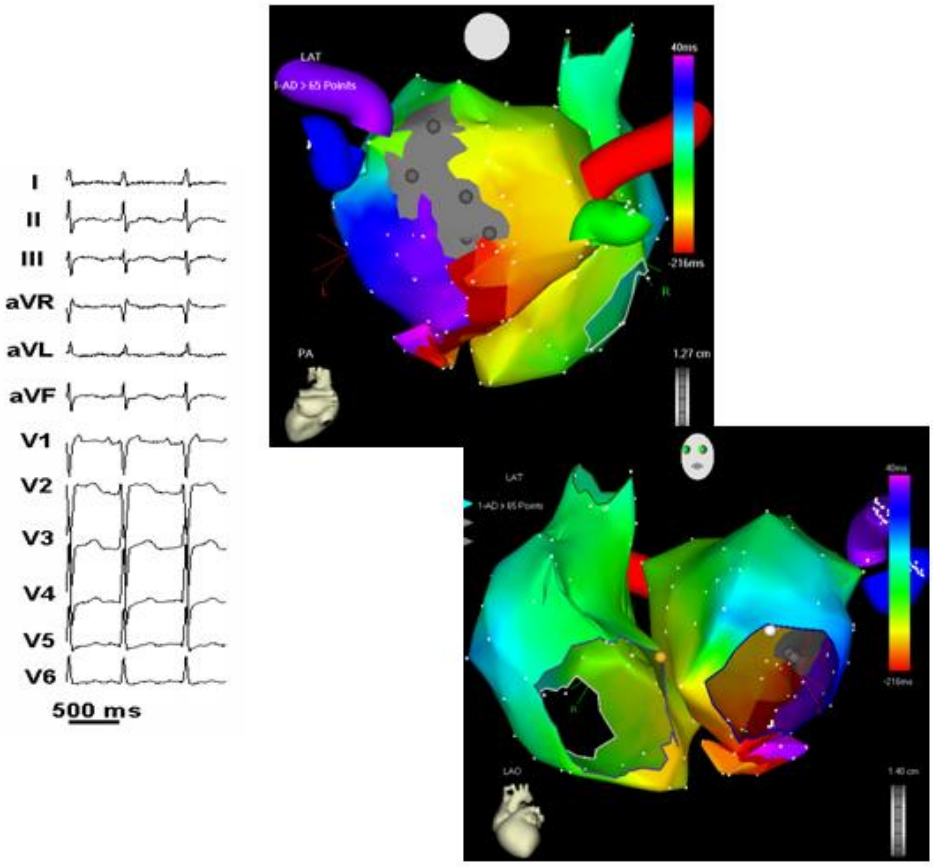

Figura 12. Activation electroanatomic mapping of a recurrent atrial flutter with 2:1 atrio-ventricular conduction, arisen after left atrial ablation for atrial fibrillation

4.5 Follow-up

During follow-up, patients remained off drugs, unless antiarrhythmic therapy was required for other arrhythmias. Patients underwent visits that included 12-lead 24-hour Holter monitoring, at 1, 3, 6 months after discharge and, subsequently, every 6 months and in case of symptom recurrences.

4.6 Statistics

Continuous variables are expressed as mean ± SD, while categorical variables are expressed as percentage. Student *t*-test or nonparametric tests (when Gaussian distribution was not confirmed) were applied to compare continuous variable. Fisher's exact test was used to define significance between frequencies. Correlation between nonnormal variables was evidenced by Spearman rank test. Odds ratio was calculated by univariate logistic regression. Sensitivity and specificity of each variable was represented by receiver operating characteristic (ROC) curves. Results from multivariate general regression were exposed with Pareto chart model. A value of $P < 0.05$ was considered statistically significant.

5. RESULTS

PART I

5.1 Patient population 1, mapping and ablation data

In part I of our search, 52 patients (37 male, 15 female; mean age 64 ± 16) were included. Twenty patients had a history of atrial fibrillation, previously treated by ablation in the left atrium in 9. Structural heart disease was present in 43 patients (83%), and 25 patients (48%) had previously undergone cardiac surgery. Fifty-six morphology of spontaneous or induced MRAT with a mean cycle length (CL) of 298 ± 76 ms were observed. 97 ± 3% of the reentry course was reconstructed by EAM, on average. In 25 morphologies (47%), the reentrant circuit was right-sided; 32 morphologies (57%) showed a double-loop reentry, with both loops sharing the same MDI in all cases. In all morphologies, the MDI was the ablation target and its location is shown in Table 1.

Location of the MDI for Each of the 56 MRAT Morphologies

Right atrium	25
Lateral wall	15
Cavotricuspid isthmus	5
Right septum	4
Posterior wall	1
Left atrium	31
Roof-anterior wall	17
Area of the right pulmonary veins	5
Area of the left pulmonary veins	2
Left septum	3
Posterior wall	3
Mitral isthmus	1

Table 1

Conduction velocity (CV) across the MDI was significantly slower than in the outer loop of the reentry circuit. CV across MDI showed a weak direct correlation with the MDI width and a stronger one with its biVolt amplitude. MRAT cycle length (CL) was inversely correlated with CV across MDI. Conversely, no significant relation was observed between CV across the MDI and atrial volume and between atrial volume and the CL. Fifty-one morphologies (91%) were successfully treated during a single procedure. An example is shown in fig.13.

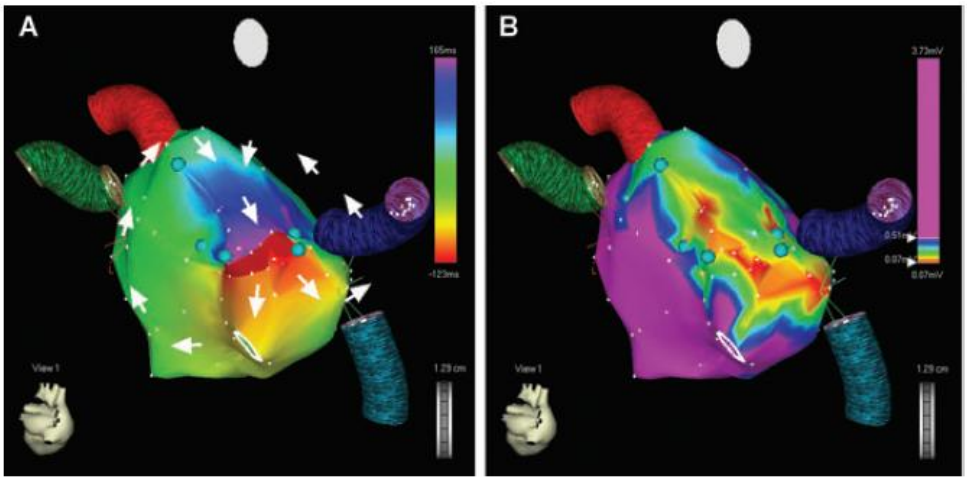

Fig . 13 Electroanatomic activation (A) and biVolt (B) maps of the left atrium during 290-ms CL MRAT successfully treated by ablation. A posterior cranialized view is shown. The activation map shows the entire reentry course; the arrows help identify the course of each loop in this double-loop reentry. The MDI is identified by the dark red band interposed between the red and purple colors; blue dots indicate sites of double potentials. In the biVolt map, the upper limit of the color-coded scale has been set at 0.5 mV to discriminate area of preserved voltage (purple) from low voltage areas (red to blue). (A) The activation map shows a double-loop reentry with both loops sharing the same MDI, between 2 lines of double potentials in the superomedial left atrium. The MDI width is 20 mm and crowding of colors indicates slow conduction (30 cm/sec) in the MDI. (B) The MDI shows low biVolt amplitude. The MDI was persistently blocked by 8 radiofrequency energy applications, with tachycardia termination, and favorable outcome.

Five left MRAT were unsuccessfully treated at the MDI. After failure, further analysis of the EAM confirmed that alternative isthmi were less suitable for

ablation than the MDI in all 5 cases and, therefore, ablation of alternative isthmi was not attempted. During the follow-up, 4 patients had recurrences of MRAT. Three had a persistent recurrence of the same morphology within the first month after ablation and retreatment was offered: 1 patient refused and 2 accepted and the same tachycardia circuit was ablated. The fourth patient had a late recurrence (> 6 months) with a different morphology and CL; a second procedure identified a new tachycardia circuit, which was successfully ablated.

5.2 Comparison of the successfully and unsuccessfully cases in population 1: identification of independent predictors of acute and/or cumulative failure

Figure 14 shows the correlation between MDI CV and width for each morphology, according to acute success, success with early recurrence of the same morphology, and failure.

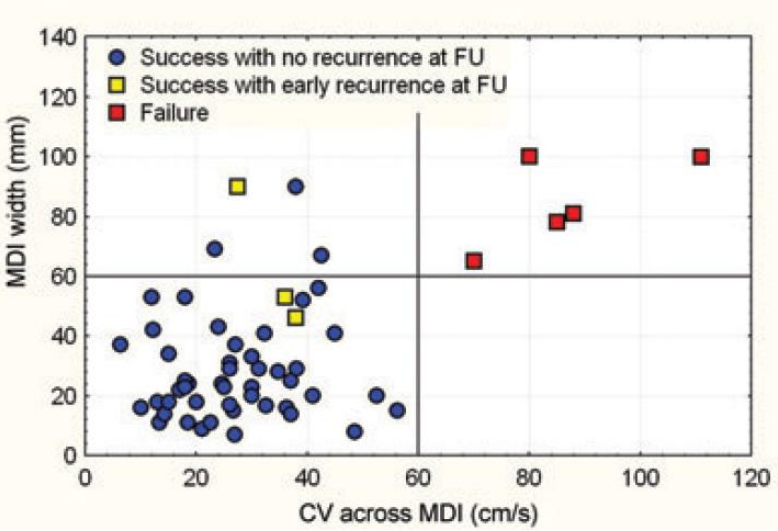

Fig. 14. CV and MDI width in population 1

In 33 of 56 morphologies (59%), MDI CV and width were below 40 cm/sec and 40 mm, respectively. All these morphologies were ablated successfully with no recurrence, using a lower number of radiofrequency applications as compared to the remaining morphologies. In the 18 of 56 morphologies (32%) with a CV across the MDI < 60 cm and a MDI width > 40 mm, ablation was acutely successful in all cases, but 3 patients had an early recurrence of the same morphology accounting for a recurrence rate of 17%.

Finally, all 5 of 56 morphologies (9%) unsuccessfully treated showed a CV and width of the MDI > 60 cm/sec and 60 mm, respectively. In table 2, univariate analysis of the considered variables is shown for successfully and unsuccessfully treated morphologies. Between the two groups there was no significant difference in the considered clinical variables; conversely, there was an evident difference in the electroanatomic characteristic of the reentrant circuit. In fact, the MDI width, mean biVolt, and CV had significantly lower values in successfully treated as compared to unsuccessfully treated morphologies, while the CV over the outer loop of the reentry circuit was comparable in both groups. Other 2 variables were significantly different in the 2 groups: tachycardia CL and a left-sided location of the MRAT. The significantly longer arrhythmia CL in successfully treated cases can be attributed to the inverse relationship between the value of CV across the MDI and the MRAT CL combined with a significantly slower CV across the MDI in successfully treated MRAT (Table 2).

Clinical, Electrophysiologic, and Electroanatomic Characteristic of the Successfully and Unsuccessfully Treated Cases

	Success	Failure	P Value
Number of morphologies	51	5	–
Female	16 (31%)	0	0.172
Age (years)	63 ± 17	63 ± 18	0.984
Coronary artery disease	5 (10%)	2 (40%)	0.112
Valvular heart disease	15 (29%)	0	0.196
Congenital heart disease	8 (16%)	0	0.448
LVEF > 50%	38 (75%)	4 (80%)	0.694
Oral amiodarone	13 (25%)	2 (40%)	0.406
Atrial volume (mL)	126 ± 45	155 ± 21	0.174
MRAT CL (ms)	305 ± 76	228 ± 17	0.029
Left-sided circuit	25 (49%)	5 (100%)	0.037
Double-loop reentry	30 (59%)	2 (40%)	0.416
MDI width (mm)	31 ± 19	93 ± 29	<0.0001
CV in the MDI (cm/sec)	28 ± 12	87 ± 15	<0.0001
CV in the outer loop (cm/sec)	78 ± 20	88 ± 15	0.183
Mean biVolt in the MDI (mV)	0.29 ± 0.30	0.93 ± 0.64	0.0001

LVEF = left ventricular ejection fraction

Table 2

Mulitvariate analysis was performed and ROC curves calculated for both procedural failure and cumulative failure. At multivariate analysis, only CV and width of the MDI were strong predictors of acute failure and cumulative failure, respectively (Table 3).

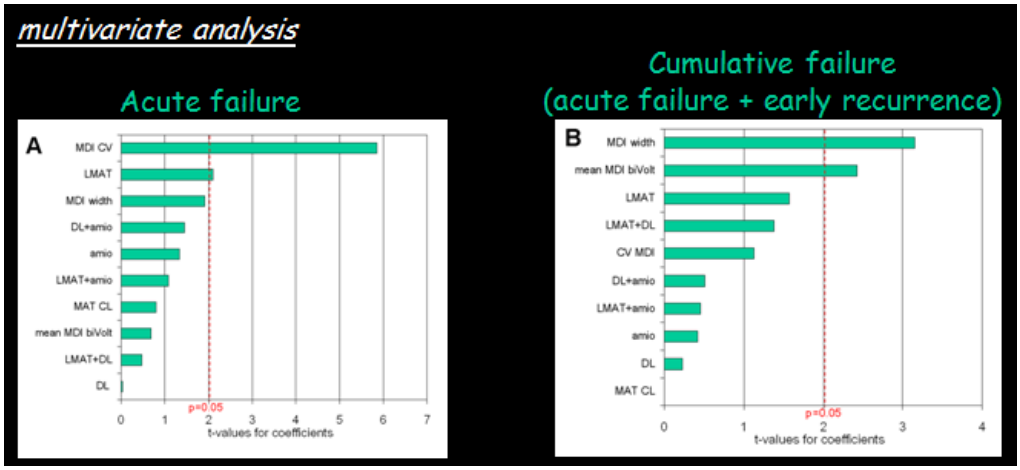

Table 3. Independent predictors of acute success or cumulative failure in population I

For procedural failure, CV was the only strong independent predictor, while a left-sided location of the MRAT showed marginal significance and all the other considered variables lost statistical significance. For cumulative failure, MDI width was the strongest independent predictor, while the mean biVolt value in the MDI had a rather marginal signifcance and all the other variables lost statistical significance. Specifically, a preserved ($\geq$ 60 cm/sec) CV in the MDI was the stronger predictor of procedural failure, while the presence of an isthmus wider than 40 mm predicted cumulative failure.

PART II

5.3 Delevopment of an algorithm to predict the difficulty of the ablation procedure

In part II of our research, we analyzed the relation between the strongest predictors of procedure outcome identified in part I (MDI width and conduction velocity in the MDI) and the chance of success of the ablation procedure, developing an algorithm to predict the difficulty of the procedure. The difficulty of the ablation was expressed by number of radiofrequency applications required to obtain conduction block. In order to test the effect of both the strongest outcome predictors of macroreentrant atrial tachycardia ablation, we applied a multiple linear regression. This multiparametric equation included the number of radiofrequency applications as dependent variable and MDI width and MDI conduction velocity as indipendent variables (table 4).

	Beta	Std err. – of beta	B	Std err. – of B	T(52)	P level
Intercept			0.745	2.540	0.293	0.770
MDI velocity (cm/s)	0.061	0.096	0.048	0.075	0.635	0.527
Isthmus width (mm)	0.774	0.096	0.513	0.064	7.999	0.000

Number of predicted RF applications:

0.048 X MDI VELOCITY + 0.513 x MDI WIDTH + 0.75

Table 4

5.4 Population II, mapping and ablation data

In the second part of the present study, 18 consecutive patients (8 males, 10 females; mean age 58 ± 19, range 21-82 years) with symptomatic sustained macroreentrant atrial tachycardias/atypical atrial flutters undergoing catheter ablation at our institution were included. We examined both spontaneous and induced macroreentrant atrial tachycardias. Patients with intracardiac thrombus detected at routine preprocedure transesophageal echocardiography and patients with absolute contraindication to oral anticoagulant or heparin were excluded. Twenty-one morphologies of atrial flutters/macroreentrant atrial tachycardias with a mean cycle of 289 ± 76 msec were studied. Structural cardiac disease was present in all patients and 12 patients (67%) had previously undergone cardiac surgery because of valvular or congenital heart disease (fig.15).

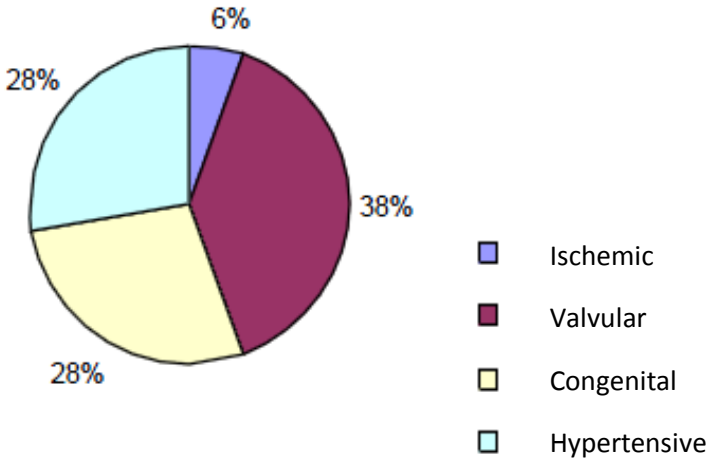

Fig. 15 Distribution of structural heart disease in population II

Antiarrhythmic therapy has not been withdrawn because not prediciting of procedural success in the first part of our research. The surface-P-wave onset has been identified for each tachycardia morphology and we consequently calculated the window of interest. In the chamber of interest, 107 ± 36 mapping sites were acquired (range 40-181 points) and 97,5 ± 3% of the reentry course was reconstructed by electroanatomic mapping, on average. The MDI has been identified in all tachycardia morphologies examined, between anatomic barriers, double potentials lines and scar areas. Location of MDI in population II is shown in table 5. Seventeen morphologies showed a double-loop reentry and four MRAT showed a single-loop reentry.

LOCATION	*N. MORPHOLOGIES*
Right atrium	***5***
Lateral wall	4
Postero-lateral wall	1
Left atrium	***16***
Roof	6
Lateral	2
Medial	2
Anterior	1
Left septum	1
Posterior wall	4

Table 5. Location of MRAT mid-diastolic isthmus in population II

The width of MDI was 38,7 ± 21,7 mm on average (range 7-87 mm), conduction velocity (CV) across the MDI was 39 ± 18,8 cm/sec and MDI mean biVolt was 0,37 ± 0,39 mV. Electroanatomic characteristics of population II are described in table 6.

Cycle (msec)	289 ± 76
Mapped cycle (%)	98 ± 3
Dual loop/Single loop	17/4
Chamber of interest volume (cc)	139 ± 54
N. of mapped sites	107 ± 36
MDI width (mm)	39 ± 22
CV MDI (cm/sec)	39 ± 19
Mean biVolt (mV)	0.37 ± 0.39

Table 6. Electroanatomic characteristics of population II

No intra- or post-procedural complications were observed in all treated patients. Ablation procedure was successfully completed 81% of treated morphologies. In 3 patients, a first arrhythmia morphology changed during the electroanatomic mapping in another maroreentrant tachycardia which was successfully mapped and treated. Nowadays, no recurrences of MRATs acutely successfully treated were observed.

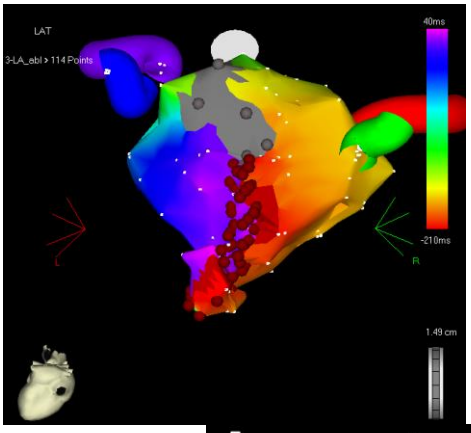

Fig.16

Left atrial activation map during left atrial flutter; red points identify the ablation line at the MDI

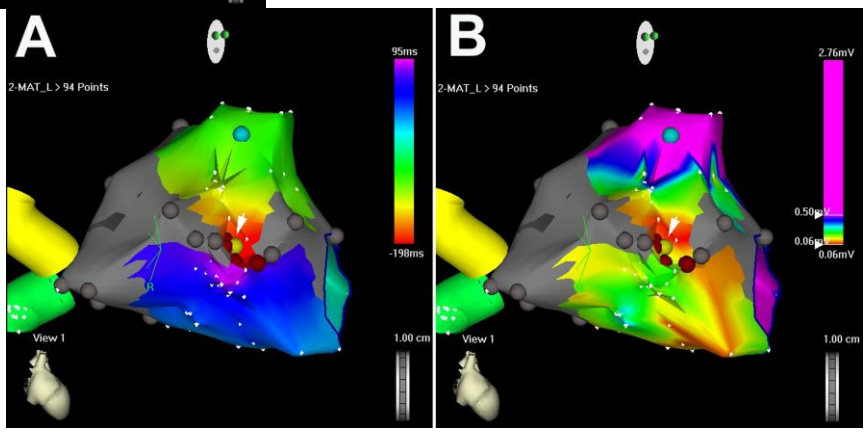

Fig. 17 A. Left MRAT activation map (cycle 300 ms) after left atrial ablation for atrial fibrillation (MDI location is site of previous linear ablation between mitral annulus and right sup.pulmonary vein.

Fig 17 B. BiVolt map: low potential identify the MDI

Population I and II did not significantly differ as to the main electroanatomic and clinical features (MDI width, CV across the MDI, MDI mean biVolt, atrial volume, arrhythmia cycle, age). Population II showed a larger percentage of patients with previous surgery history, but this variable did not affect the procedural success in neither of the populations (table 7).

Population 1 vs 2	MEAN 1	MEAN 2	STD 1	STD2	*P-VALUE*
AGE (YRS)	**61,9**	**58,2**	**16,91**	**19,00**	***0,26***
CV in the MDI (cm/sec)	**33,0**	**39,0**	**20,44**	**19,0**	***0,25***
MDI WIDTH (mm)	**35,8**	**39,0**	**26,89**	**22,0**	***0,71***
ATRIAL VOLUME (cc)	**128,1**	**139**	**44,14**	**54**	***0,42***
CL (ms)	**297,2**	**289**	**76,01**	**76**	***0,70***
MEAN Bi-VOLT (mV)	**0,34**	**0,37**	**0,31**	**0,39**	***0,62***

Table 7. Electroanatomic and clinical features of population I and II

As previously observed in population I, MDI width and conduction velocity across the MDI were the most significant predictors of procedural success. BiVolt amplitude, even if because of a little difference, did not reach the statistical significancy (table 8).

	Success	*Failure*	*P-value*
N. of morphologies	**17**	**4**	
Atrial volume (cc)	**129 ± 50**	**177 ± 61**	**0,116**
Cycle (msec)	**300 ± 80**	**240 ± 20**	**0,162**
MDI vel (cm/sec)	**33 ± 12**	**66 ± 20**	**< 0,001**
MDI width (mm)	**31 ± 14**	**73 ± 11**	**< 0,001**
BiVolt amplitude (mV)	**0.29 ± 0.18**	**0.7 ± 0.8**	**0,052**

Table 8. Ablation procedure outcome in population II

As we observed in population I, also in the second population MDI width > 60 mm and a conduction velocity across the MDI > 60 cm/s were strongly associated with procedural failure (fig. 18).

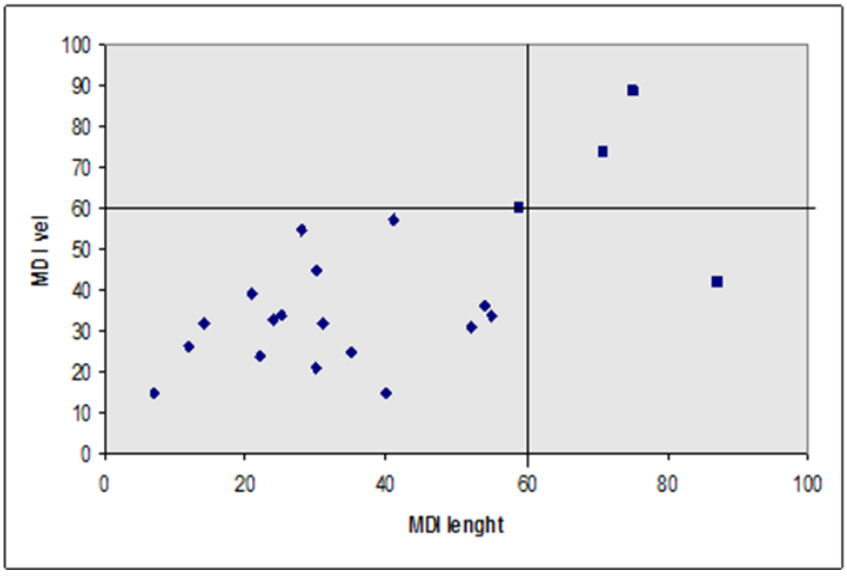

Fig. 18 Ablation outcome in population II: MDI width and MDI conduction velocity confirmed to be strong predictors of failure

5.5 Validation of the algorithm to predict the difficulty of ablation of macroreentrant atrial tachycardia

In order to test the effect of both the strongest outcome predictors (MDI width and CV across the isthmus) of macroreentrant atrial tachycardia ablation, we applied a multiple linear regression. The difficulty of ablation procedure was expressed by number of radiofrequency applications required to obtain conduction block at the MDI (target of procedure). This multiparametric equation included the number of radiofrequency applications as dependent variable and MDI width and MDI conduction velocity as indipendent variables. Excluded possible bias, we applied a linear regression to both the populations one by one and subsequently taken together in order to verify the reliability of the regression itself (fig. 19 A e B).

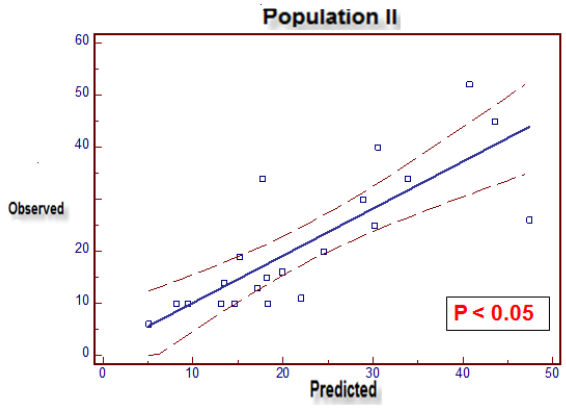

Fig. 19A

Population I

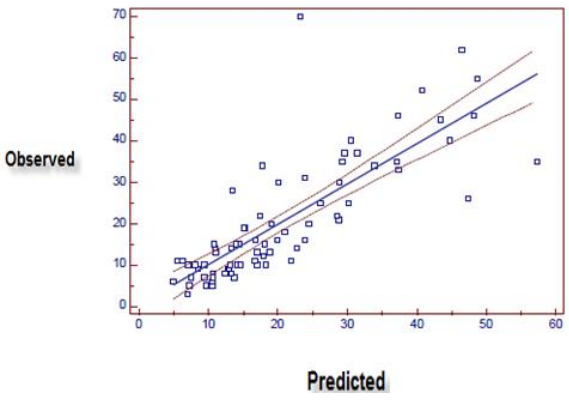

Fig. 19B

Population I + II

In comparison with the predicted number of radiofrequency applications, the linear regression demonstrated to be reliable; it was in error for a number of 10 applications in 90% of examined cases and its error was independent from all the observed variables (fig. 20). The regression reliability decreases as the error tolerance decreases (if we accept an error of seven applications in comparison with the predicted number, the linear regression demonstrates reliability equal to 82%).

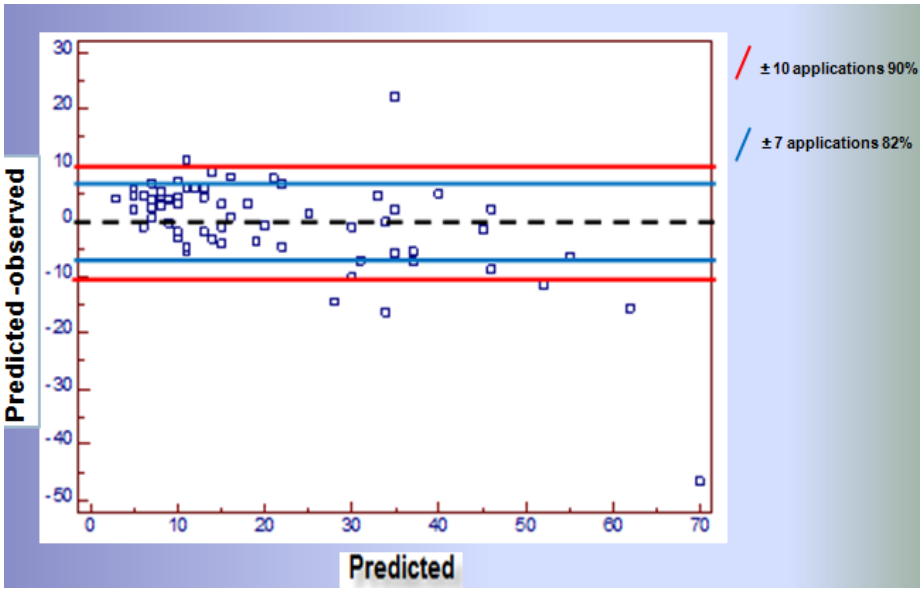

Fig. 20 Difference between predicted and observed

6. DISCUSSION

Although its exact prevalence among cardiac arrhythmias is difficult to establish clinically, MRAT is not a rare arrhythmia. In patients with complex anatomy and multiple reentrant loops, it may be difficult to clarify the atrial activation during MRAT in order to define a rational ablation strategy. To this purpose, 3-dimensional electroanatomic mapping (EAM) proved very effective. However ablation of this arrhythmias remains challenging and sometimes it may results in a lenghty procedure or failure. In previous mono- and multi-centric experiences[13,15], the ablation linearly placed at the mid-diastolic isthmus (MDI) achieved arrhythmia interruption and conduction block in the great part of cases. Shah et al. demonstrated that left macroreentrant atrial tachycardias after ablation for atrial fibrillation are characterized by a narrow mid-diastolic activation isthmus and a slow conduction velocity across the mid-diastolic isthmus and they can be effectively treated with radiofrequency ablation having the isthmus of the reentry as procedural target[41]. The first part of our research (subject of a publication) identified, for the first time, some electronatomic variables as ablation adverse outcome predictors[42]. However, all the published studies up to today agree identifing the mid-diastolic activation isthmus as the critical part of the reentry.

If the electroanatomic mapping identifies a mid-diastolic activation isthmus (the “fragile” portion of the macroreentry) characterized by a significantly slow velocity of conduction and a small widht, the ablation outcome will be most likely favourable. The macroreentrant arrhythmias characterized by a

preserved conduction velocity in every part of the circuit or characterized by a particularly wide isthmus, a stable interruption of the arrhythmia through radiofrequency applications will be very unlikely and a procedural failure will be likely.

Our research present some limitations. The conduction velocity was calculated manually, while a trigonometric method is more accurate to quantify the wavefront propagation velocity[40]. However, manual method has been already used to calculate conduction velocity in several atrial regions[43]. Moreover, in our research, particular care was taken to define the direction of propagation and to avoid curvilinear areas, where estimate of the true distance between 2 sites may be inaccurate on electroanatomic mapping. The reliability of the model studied still present some limitations, because it's not able to exactly predict the procedural difficulty. The inaccuracy of the algorithm probalbly depends on the limited number of the variables included in the linear regression model (beacuse of their statistical relevance) which can not express the entire ablation complexity.

An increase of the accuracy of the algorithm could be reached increasing the number of examined cases in order to include further variables in the linear regression model (for example, mean biVolt amplitude of the mid-diastolic isthmus, very close to statistical significancy in our study).

7. REFERENCES

[1] Anderson RH, Ho SY. The architecture of the sinus node, the atrioventricular conduction axis, and the internodal atrial myocardium. J. Cardiovasc. Electrophysiol. 1998; 9: 1233-48

[2] Tawara S. Das Reitzleitungssystem des Saűgetierherzen. G. Fisher, Jena 1906

[3] Koch W. Weiter Mitteilungen uber den Sinusknoten der Herzens. Verhandlungen der Deutschen Pathologische Anatomie 1909; 13: 85-92

[4] Keith A, Flack MW. The auricolo-ventricular bundle of the human heart. Lancet 1906; 2:359-64

[5] Triedman JK, Saul JP, Weindling SN, et al. Radiofrequency ablation of intraatrial reentrant tachycardia after surgical palliation of congenital heart disease. Circulation 1995; 91: 707-14

[6] Gerstenfeld EP, Callans DJ, Dixit S, et al. Mechanisms of organized left atrial tachycardias occurring after pulmonary vein isolation. Circulation 2004; 110: 1351-57

[7] Ho SY, Sanchez-Quintana D, Cabrera JA, et al. Anatomy of the left atrium: implications for radiofrequency ablation of atrial fibrillation. J Cardiovasc Electrophysiol 1999; 10: 1525-33

[8] Nathan H, Eliakin M. The junction between the left atrium and the pulmonary veins. Circulation 1966; 34: 412-21

[9] Zipes DP, Knope RF Electrical properties of the thoracic veins. Am J Cardiol 1972; 29: 372-6

[10] Schamroth L. The Disorders of Cardiac Rhythm. Blackwell, Oxford, 1971, p. 49

[11] Saoudi N, Cosio F, Waldo A, et al. A classification of atrial flutter and regular atrial tachycardia according to electrophysiological mechanisms and

anatomical bases; a Statement from a Joint Expert Group from the Working Group of Arrhythmias of the European Society of Cardiology and the North American Society of Pacing and Electrophysiology. Eur Heart J 2001; 22 (14): 1162-82

12 Lesh MD, Van Hare GF, Epstein LM, et al. Radiofrequency catheter ablation of atrial arrhythmias: results and mechanisms. Circulation 1994; 89: 1074-89

13 Jais P, Shah DC, Haissaguerre M, et al. Mapping and ablation of atypical left atrial flutters. Circulation 2000; 101: 2928-34

14 Triedman JK, Alexander ME, Love BA, et al. Influence of patient factors and ablative technologies on outcome of radiofrequency ablation of intra-atrial re-entrant tachycardia in patients with congenital heart disease. J Am Coll Cardiol 2002; 39: 1827-35

15 De Ponti R, Verlato R, Bertaglia E, et al. Treatment of macro-re-entrant atrial tachycardia based on electroanatomic mapping: Identification and ablation of the mid-diastolic-isthmus. Europace 2007; 9: 449-57

16 Rosenblueth A, Garcia-Ramos J. The influence of artificial obstacles on experimental auricular flutter. Am Heart J 1947; 33: 677-84

17 Frame LH, Page RL, Boyden PA, et al. Circus movement in the canine atrium around the tricuspid ring during experimental atrial flutter and during reentry in vitro. Circulation 1987; 76: 1155-75

18 Boyden PA, Frame LH, Hoffman BF. Activation mapping of reentry around an anatomic barrier in the canine atrium: observations during entrainment and termination. Circulation 1989; 79:406-16

19 Schoels W, Kuebler W, Yang H, et al. A unified functional/anatomic substrate for circus movement atrial flutter: activation and refractory patterns

in the canine right atrial enlargement model. J Am Coll Cardiol 1993; 21: 73-84

[20] Feld GK, Shahandeh RF. Activation patterns in experimental canine atrial flutter produced by right atrial crush injury. J Am Coll Cardiol 1992; 20: 441-51

[21] Cosio FG, Lopez GM, Goicolea A, et al. Electrophysiologic studies in atrial flutter. Clin Cardiol 1992; 15: 667-73

[22] Olshansky B, Wilber DJ, Hariman RJ. Atrial flutter: update on the mechanism and treatment. PACE. Pacing Clin Electrophysiol 1992: 15: 2308-35

[23] Waldo AL. Atrial flutter : new directions in management and mechanism. Circulation 1990; 81: 1142-3

[24] Feld GK, Fleck RP, Chen PS, et al. Radiofrequency catheter ablation for the treatment of the human type I atrial flutter: identification of a critical zone in the reentrant circuit by endocardial mapping techinques. Circulation 1992; 86: 1233-40

[25] Olshansky B, Okumura K, Hess PG, et al. Demonstration of an area of slow conduction in human atrial flutter. J Am Coll Cardiol 1990; 16: 1639-48

[26] Touboul P, Saoudi N, Atallah G, et al. Electrophysiologic basis of catheter ablation in atrial flutter. Am J Cardiol 1989; 64: 795-825

[27] Nakagawa H, Wang X, McClelland J, et al. Line of conduction block extends from inferior vena cava to coronary sinus ostium in common atrial flutter. PACE Pacing Clin Electrophysiol 1993; 16: 881

[28] Saoudi N, Atallah G, Kirkorian G, et al. Catheter ablation of the atrial myocardium in human type I flutter. Circulation 1990; 81: 762-71

[29] Calkins H, Leon AR, deam AG, et al. Catheter ablation of atrial flutter using radiofrequency energy. Am J Cardiol 1994; 73: 353-6

[30] Interian AJ, Cox MM, Jimenez RA, et al. A shared pathway in atrioventricular nodal reentrant tachycardia and atrial flutter: implications for pathophysiology and therapy. Am J Cardiol 1993; 71: 297-303

[31] Lesh MD, Van Hare GF, Fitzpatrick Ap, et al. Curing reentrant atrial arrhythmias: targeting protected zones of slow conduction by catheter ablation. J Electrocardiol 1993; 26: 194-203

[32] Yamauchi S, Schuessler RB, Kawamoto T, et al. Use of intraoperative mapping to optimize surgical ablation of atrial flutter. Ann Thorac Surg 1993; 56: 337-42

[33] Olgin JE, Kalman JM, Fitzpatrick AP, et al. Role of atrial endocardial structures as barriers to conduction during human type I atrial flutter. Circulation 1995; 92: 1839-48

[34] Cosio FG, Lopez GM, Goicolea A, et al. Radiofrequency ablation of the inferior vena cava-tricuspid valve isthmus in common atrial flutter. Am J Cardiol 1993; 71: 705-9

[35] Gepstein L, Hayam G, Ben-Haim S. A novel method for nonfluoroscopic catheter-based electroanatomical mapping of the heart. In vitro and in vivo accuracy results. Circulation 1997; 95: 1611-22

[36] Hayam G, Gepstein L, Ben-Haim S. Accuracy of the in vivo determination of location using a new nonfluoroscopic electroanatomical mapping system. PACE [Abstract] 1996. 19:712

[37] Smeets J, Ben-Haim S, Rodriguez L, et al. New method for nonfluoroscopic endocardial mapping in humans. Accuracy assessment and first clinical

results. Circulation 1998. 97: 2426-32

[38] Spach MS, Lieberman M, Scott JG, et al. Excitation sequences of the atrial septum and the AV node in isolated hearts of the dog and rabbit. Circ Res 1971; 29: 156-72

[39] Harrild DM, Henriquez CS. A computer model of normal conduction in the human atria. Circ Res 2000; 87: e25-e36.

[40] Kojodjojo P, Kanagaranam P, Markides V, et al. Age-related changes in human left and right atrial conduction. J Cardiovasc Electrophysiol 2006; 17: 120-127

[41] **S**hah D, Sunthorn H, Burri H, et al. Narrow, slow-conducting isthmus dependent left atrial reentry developing after ablation for atrial fibrillation: ECG characterization and elimination by focal RF ablation. J Cardiovasc Electrophysiol 2006; 17: 516-9

[42] De Ponti R, Marazzi R, Zoli L et al. Electroanatomic Mapping and ablation of Macroreentrant Atrial Tachycardia: Comparison between successfully and unsuccessfully treated cases J Cardiovasc Electrophysiol 2010; 21: 155-62

[43] Sanders P, Morton JB, Davidson NC, et al. Electrical remodeling of the atria in congestive heart failure: electrophysiological and electroanatomic mapping in humans. Circulation 2003: 108; 1461-8

8. Acknowledgements

I'm very grateful to my Professor Jorge A. Salerno-Uriarte, Professor Daniela Negrini and Professor Roberto De Ponti, for continuous advice, support, trust and for the precious scientific discussions during these years.

A particular acknowledgement to Dr. Raffaella Marazzi for the precious suggestions and advices.

9. Contributions

The results obtained in the present research project, have contributed to the publication of the following scientific manuscript:

- De Ponti R, Marazzi R, Zoli L et al. Electroanatomic Mapping and ablation of Macroreentrant Atrial Tachycardia: Comparison between successfully and unsuccessfully treated cases *J Cardiovasc Electrophysiol 2010; 21: 155-62*

In addition the data of this research have been presented in national scientific meetings:

- Zoli L Electroanatomic mapping of atrial macro-reentry. First Meeting of the Italian Council of PhD Fellows, Erice, November 7th - 8th, 2010

- Zoli L, De Ponti R, Marazzi R et al. Electroanatomic mapping and ablation of macroreentrant atrial tachycardia. Poster session, I Riunione scientifica dei Dottorandi di ricerca dell'Università dell'Insubria, Castel Ivano, Ottobre 2010